JOURNAL OF CATALYSIS 146, 155–165 (1994)

Characterization of the Acidic and Basic Properties of $\alpha LiAlO_2$, $\gamma LiAlO_2$, and Calcined "$HAlO_2$" Using Isopropyl Alcohol

D. C. Tomczak, J. L. Allen, and K. R. Poeppelmeier[1]

Department of Chemistry and Ipatieff Catalytic Laboratory, Northwestern University, Evanston, Illinois 60208

Received March 23, 1993; revised September 3, 1993

Characterization of both the acidic and basic sites of $\alpha LiAlO_2$, $\gamma LiAlO_2$, and calcined "$HAlO_2$" was carried out with the isopropyl alcohol probe reaction. All three materials catalyzed the formation of both propylene and acetone. The formation of propylene is indicative of acidic–basic pair sites, while the presence of acetone is indicative of basic sites. In addition to the formation of both propylene and acetone, base-catalyzed acetone aldol condensation products were formed on both $\alpha LiAlO_2$ and calcined "$HAlO_2$." Both materials produced a C6DIENE (2-methyl-1,3-pentadiene or 4-methyl-1,3-pentadiene) aldol condensation product, while $\alpha LiAlO_2$ also produced the aldol condensation products 4M2PONE (4-methyl-2-pentanone) and 4M2POL (4-methyl-2-pentanol). The reaction pathways that describe the formation of the various C6 products were used to infer the nature of the basic sites on the materials. Additional information obtained from TPD and FTIR of chemisorbed CO_2 demonstrate that the basic sites on $\alpha LiAlO_2$ are similar in strength and number to MgO. © 1994 Academic Press, Inc.

INTRODUCTION

We report the results from the catalytic characterization of both the acidic and basic properties of $\alpha LiAlO_2$, $\gamma LiAlO_2$, and calcined "$HAlO_2$." Calcined "$HAlO_2$," a lithiated γ-alumina-like material, was prepared from the precursor "$HAlO_2$," which was synthesized from $\alpha LiAlO_2$ (1–3) by "chimie douce" (soft chemistry) methods (4). The probe molecule used for the catalytic characterization was isopropyl alcohol (IPA). The conversion of isopropyl alcohol to propylene (dehydration) requires the participation of both acidic and basic sites (5), whereas the formation of acetone (dehydrogenation) is a base-catalyzed process (6–8). We report three comparisons. First, a comparison of isopropyl alcohol selectivity and activity data obtained over $\alpha LiAlO_2$ and $\gamma LiAlO_2$ provides information about the effects of cation coordination on acidity and basicity. The effects of alkali metal cation concentration on the base-catalyzed (alcohol dehydrogenation and aldol condensation) reactions are examined in the comparison of activity and selectivity data of $\alpha LiAlO_2$ and calcined "$HAlO_2$." In the third comparison, activity and selectivity data of calcined "$HAlO_2$" and γ-alumina are used to examine the effects of alkali metal cation concentration on the catalytic dehydration of alcohols. Fourier transform infrared spectroscopy (FTIR) and the desorption of chemisorbed CO_2 (TPD) have been used to characterize the coordination of CO_2 and the strength and number of basic surface sites. Both techniques (9, 10) complement the characterization of surfaces with organic probe molecules.

EXPERIMENTAL

Synthesis

$\alpha LiAlO_2$ ($R\bar{3}m$, rhombohedral, a_H = 2.8034(3) Å and c_H = 14.228(2) Å) (11) was prepared by reacting stoichiometric amounts of high surface area gelatinous boehmite ($AlO(OH) \cdot nH_2O$, 99.4 + %, 0.10 wt% Na_2O, 0.08 wt% Fe_2O_3, BET SA = 208 m^2/g, Kaiser Chemical) and Li_2CO_3 (99 + %, 0.01 wt% CaO, 0.003 wt% Fe_2O_3, 0.01 wt % K_2O, and 0.10 wt% Na_2O, Aldrich Chemical) at 600°C for a period of 2–3 days in an open air muffle furnace (1). $\gamma LiAlO_2$ ($P4_12_12$, tetragonal, a = 5.169(2) Å and c = 6.268(2) Å) (12) was prepared from the same reactants used above. The two reactants were heated to 500°C and the temperature was held constant for 24 hr. At the completion of this thermal treatment, the sample was then heated to 1000°C and the temperature was again held constant for 24 hr (2).

The precursor, "$HAlO_2$" ($Li_{1-x}H_xAlO_2$; x = 0.90), was synthesized by stirring $\alpha LiAlO_2$ in a 5 to 10 molar excess of lauric acid ($CH_3(CH_2)_{10}CO_2H$) for a period of 40 hr at 220°C under a flow of nitrogen (3). The nitrogen atmosphere suppresses lauric acid decomposition at elevated temperatures. Upon completion of the reaction, the molten lauric acid was decanted and the solid product was washed with acetone. Next, the product mixture was stirred in 8 M HNO_3 for 30 min to form a mixture of

[1] To whom correspondence should be addressed.

0021-9517/94 $6.00
Copyright © 1994 by Academic Press, Inc.
All rights of reproduction in any form reserved.

TABLE 1

Surface Area and Base Site Density (BSD) Data

Catalyst	SA (m^2/g)	BSD (10^{-6} mole/m^2)[a]
$\alpha LiAlO_2$	40	5.2
$\gamma LiAlO_2$	7	1.7
"$HAlO_2$"	39	—
Cal "$HAlO_2$"	60	1.2
γ-Alumina	200	—

[a] Determined by the BET method except for $\gamma LiAlO_2$ which was determined by the *t*-plot method.

"$HAlO_2$" (not affected by nitric acid at these conditions), lauric acid, and lithium nitrate (aq). The aqueous solution was removed and the product mixture was again washed with acetone. Both thermogravimetric and atomic absorption analysis methods were used to determine the degree of cation replacement. Calcined "$HAlO_2$" was prepared by calcining "$HAlO_2$" for a period of 4 hr at 450°C in an open air muffle furnace. XRD characterization of "$HAlO_2$" and calcined "$HAlO_2$" indicated that both materials have a spinel-like structure similar to γ-alumina. A detailed discussion of the structure is presented elsewhere (1–3, 13, 14).

High purity γ-alumina was prepared from high surface area gelatinous boehmite (Kaiser Chemical alumina source used above). The gelatinous boehmite was calcined at 400°C in an open air muffle furnace for 70 hr.

Instrumental

X-ray powder diffraction was used to identify each catalyst and to determine phase purity. Surface areas were determined from BET (15) or *t*-plot (16) analyses of nitrogen adsorption isotherms collected in a dynamic mode. The surface areas of each catalyst are shown in Table 1.

A continuous flow fixed bed reactor system equipped with a glass reactor was used for catalytic characterization. All experiments were carried out at a total pressure of 1 atm. The carrier gas for the isopropyl alcohol (IPA) feed was helium (Linde High Purity Grade, 99.995%, further purified with both a MnO oxygen trap and a 77-K activated silica gel trap). Mixing of the carrier and feed gas was achieved with a gas–liquid saturator. Both concentration and flow rate parameters of the feed gas are described in terms of gas hourly space velocities (GHSV), which are defined as

(volume of gaseous feed)/(volume of catalyst · hr).

The experimental parameters for each GHSV are shown in Table 2. An investigation of reactor background activity was carried out over the temperature range 200–425°C at an IPA partial pressure of 0.13 atm. The results indicated that the maximum operating temperature for the analyses was 325°C. At this temperature and pressure, conversion was 1.2% with 100% selectivity for propylene.

One cm^3 of 30–40 mesh sample was charged into the reactor for each experiment except for $\gamma LiAlO_2$ where 2.0 cm^3 of sample were used because of its low surface area. Prior to every experiment, each catalyst except for "$HAlO_2$" was pretreated *in situ* at 400°C for a period of 2 hr in a stream of helium. At the end of an experiment, the catalyst was cleaned of carbonaceous residue by heating to 400°C and holding the temperature for 2 hr (10% oxygen in helium).

Conversions and selectivities for each catalyst were recorded after 1.0–1.5 hr of run time at each temperature and space velocity. To compare catalyst activities, conversion data collected at similar space velocities and temperatures were used. Selectivity patterns were compared at similar conversions and temperatures except where otherwise stated. The selectivities are defined as the percentage of converted IPA which produces a specific product.

Quantitative analyses of product mixtures were conducted with a gas chromatograph (HP 5840A) equipped with a 20 ft. 10% Carbowax 20M column and a TC detector. Gas chromatography/mass spectroscopy analyses (performed by the Analytical Services Laboratories of Northwestern University) of product mixtures (condensed in a liquid-nitrogen trap) were used to identify various components.

Temperature-programmed desorption (TPD) of chemisorbed CO_2 was used to estimate base site density on the surface of the catalysts. The TCD cell of a modified Hewlett–Packard 5840A GC was used to monitor the desorption of CO_2. Approximately 450 mg of each catalyst

TABLE 2

Experimental Parameters for GHSVs Used in the IPA Probe Reaction Studies

GHSV (hr^{-1})	Catalyst (amt. used, g)	P_{IPA}	P_{He}	Sat. temp.	Total flow
36	B (1.72)	0.06	0.94	30.5	19.8
61	C (0.64)	0.06	0.94	30.0	17.0
71	A (0.79)	0.06	0.94	30.0	19.8
83	B (1.72)	0.14	0.86	43.0	19.8
84	D (0.43)	0.07	0.93	32.0	20.0
140	A (0.79)	0.12	0.88	41.0	19.4
148	C (0.64)	0.15	0.85	43.0	16.4
186	B (1.72)	0.34	0.66	64.0	18.2
372	C (0.64)	0.35	0.65	62.5	17.7
407	A (0.79)	0.15	0.85	45.0	45.2
900	A (0.79)	0.32	0.68	60.0	46.9

Note. Units: Pressure (atm), temperature (°C), and flow rate (cm^3/min). A = $\alpha LiAlO_2$, B = $\gamma LiAlO_2$, C = Calcined "$HAlO_2$," and D = γ-alumina.

TABLE 3

Selectivity and Activity Data for $\alpha LiAlO_2$

GHSV (hr^{-1})	PROP	ACET	C6DIENE	4M2PONE	4M2POL	AP	Conv. (%)
			At 300°C				
71	7.4	17.6	6.0	4.5	26.3	38.2	33.9
140	6.3	21.9	9.4	2.2	33.2	27.0	15.6
407	4.2	25.8	9.0	1.6	35.4	24.0	10.6
900	5.3	29.2	12.0	0.0	16.5	37.0	3.4
			At 325°C				
71	8.0	16.8	7.2	7.4	17.0	43.6	54.3
140	3.4	19.3	6.9	6.2	27.1	37.1	39.6
407	3.5	20.5	7.0	5.2	34.6	29.2	27.2
900	4.0	25.2	9.0	2.3	34.3	25.2	13.4

was pretreated at 400°C for 2 hr in a 30 cm^3/min flow of helium and then was cooled to room temperature. CO_2 (Linde Instrument Grade, 99.99%) was passed over each sample for 12 hr at a rate of 30 cm^3/min. Physisorbed CO_2 was removed with a 2-hr purge of helium at 50 cm^3/min. After this purge, the temperature of the system was increased linearly at a rate of 10°C/min to a maximum temperature of 500°C. The data were quantified by comparing observed peak areas with peak areas from the decomposition of known amounts of $PbCO_3$.

An infrared spectrum of CO_2 adsorbed on $\alpha LiAlO_2$ was obtained with a Nicolet FTIR spectrometer. The sample was pressed (9000 psi) into a self-supporting wafer using a stainless steel die. The wafer was mounted in a controlled atmosphere cell equipped with a pretreatment furnace. The sample was pretreated at 500°C under a flow of argon (Linde High Purity Grade, 99.996% 30 cm^3/min) for 1 hr, then cooled to 25°C. The atmosphere was switched to a flow of CO_2 (30 cm^3/min) for a period of 2 hr. Next, the cell was purged with argon for 30 min and the interferograms were recorded.

RESULTS

The results from the catalytic characterization of $\alpha LiAlO_2$ and $\gamma LiAlO_2$ with IPA are presented in Tables 3 and 4. Both $\alpha LiAlO_2$ and $\gamma LiAlO_2$ produced the commonly observed products of propylene and acetone (17, 18). However, additional products were observed on $\alpha LiAlO_2$. The list of additional products is comprised of diacetone alcohol (DAA), mesityl oxide (MO), 4-methyl-2-pentanol (4M2POL), 4-methyl-2-pentanone (4M2PONE), and 2-methyl-1,3-pentadiene or 4-methyl-1,3-pentadiene (C6DIENE). In this paper, these products are collectively referred to as C6.

Aldol condensation of acetone results in the formation of DAA, which, in turn, rapidly undergoes dehydration to generate MO. The selectivities for DAA and MO are not tabulated because they were only observed in trace quantities. The column labeled AP in Tables 3–6 represents the amount of IPA not accounted for in a carbon balance. Most of this "lost" carbon is probably present in the condensed material observed on the internal surfaces of the reactor. This condensed material consists of high molecular weight products (>C6) that form as a result of aldol condensation reactions involving MO and 4M2PONE.

IPA conversion and selectivity data of calcined "$HAlO_2$" are presented in Table 5. The selectivity data of calcined "$HAlO_2$" show the formation of a smaller amount of AP compared to $\alpha LiAlO_2$. The selectivity data also show little dehydration activity relative to γ-alumina.

High purity γ-alumina was chosen as a reference material for IPA dehydration because it is known to be an

TABLE 4

Selectivity and Activity Data for $\gamma LiAlO_2$ at 325°C

GHSV (hr^{-1})	PROP	ACET	C6DIENE	4M2PONE	4M2POL	AP	Conv. (%)
36	27.6	69.0	3.4	0.0	0.0	0.0	2.9
83	25.0	75.0	0.0	0.0	0.0	0.0	0.8
186	40.0	60.0	0.0	0.0	0.0	0.0	0.5

TABLE 5

Selectivity and Activity Data for Calcined "$HAlO_2$"

GHSV (hr^{-1})	PROP	ACET	C6DIENE	4M2PONE	4M2POL	AP	Conv (%)
			At 275°C				
61	33.9	66.1	0.0	0.0	0.0	0.0	1.5
			At 300°C				
61	21.5	71.4	0.0	0.0	0.0	7.1	5.9
148	22.5	61.6	0.0	0.0	0.0	15.9	2.9
372	17.4	51.2	0.0	0.0	0.0	31.4	3.2
			At 325°C				
61	13.6	65.6	11.3	0.0	0.0	9.5	21.5
148	16.3	71.9	0.0	0.0	0.0	11.8	9.4
372	13.2	59.4	1.1	0.0	0.0	26.3	9.3

extremely active and selective catalyst for secondary alcohol dehydration (5, 19). Table 6 shows the selectivity and conversion data of IPA over γ-alumina. DIPE is used as an abbreviation for diisopropyl ether. As expected, γ-alumina exhibited considerable activity at low temperatures with a high degree of selectivity towards the formation of propylene.

"$HAlO_2$" showed no activity for the conversion of IPA below 230°C. "$HAlO_2$" could not be tested at temperatures higher than 230°C because above this temperature the material undergoes dehydroxylation and converts to calcined "$HAlO_2$." Therefore, "$HAlO_2$" is not discussed in the remaining sections of the paper.

The CO_2 TPD profiles of $\alpha LiAlO_2$, calcined "$HAlO_2$," and $\gamma LiAlO_2$ are shown in Fig. 1. The profiles show a difference in the strengths of the basic sites on each of the catalysts. Each exhibits a large peak centered at 80–100°C, but only $\alpha LiAlO_2$ and calcined "$HAlO_2$" show peaks at higher temperatures which are indicative of stronger basic sites.

The amount of CO_2 desorbed from the basic sites was quantified by the integration of the observed peak areas. The number of moles of chemisorbed CO_2 divided by the surface area is the base site density. The base site densities of $\alpha LiAlO_2$, calcined "$HAlO_2$," and $\gamma LiAlO_2$ are shown in Table 1.

The infrared spectrum of adsorbed CO_2 on $\alpha LiAlO_2$ in the region of 1215–1800 cm^{-1} is shown in Fig. 2. IR bands are observed at approximately 1408, 1491, 1560, and 1645 cm^{-1}.

DISCUSSION

Catalysis Data

$\alpha LiAlO_2$ vs $\gamma LiAlO_2$. The selectivity and the activity data of IPA conversion on $\alpha LiAlO_2$ and $\gamma LiAlO_2$ provides a direct comparison of the effect of cation coordination on the acidity and basicity of the two polymorphs. All of the cations of $\alpha LiAlO_2$ are in octahedral coordination, and all of the cations of $\gamma LiAlO_2$ are in tetrahedral coordination. Examination of the conversion data presented in Fig. 3 shows $\gamma LiAlO_2$ with less activity compared to $\alpha LiAlO_2$. At 325°C and a GHSV $\approx$ 80 hr^{-1}, $\gamma LiAlO_2$ exhibited a conversion of 2.9% compared to 54.3% for $\alpha LiAlO_2$.

Information regarding the type of activity (dehydration, dehydrogenation, aldol condensation, etc.) was obtained from selectivity data collected at similar conversions and temperatures. To compare the selectivity data at a similar conversion, data sets from different temperatures were used. The selectivity data of $\alpha LiAlO_2$ were collected at 300°C and a GHSV = 900 hr^{-1}, and the selectivity data of $\gamma LiAlO_2$ were collected at 325°C and a GHSV = 36 hr^{-1}. With conversions at about 3%, comparison of the

TABLE 6

Selectivity and Activity Data for γ-Alumina at GHSV = 84 hr^{-1}

Temp. (°C)	PROP	ACET	C6DIENE	DIPE	AP	Conv. (%)
175	72.0	0.0	0.0	28.0	0.0	16.5
200	85.1	0.0	0.0	14.9	0.0	53.9
225	99.9	0.0	0.0	0.1	0.0	96.3
250	100.0	0.0	0.0	0.0	0.0	100.0

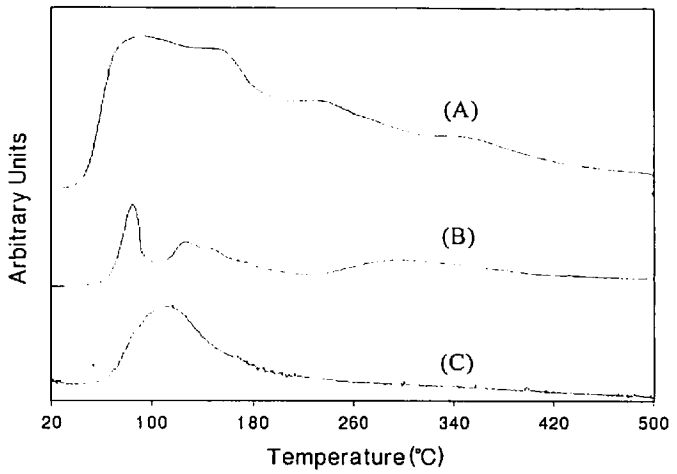

FIG. 1. The CO_2 TPD profiles of (A) $\alpha LiAlO_2$, (B) calcined "$HAlO_2$," and (C) $\gamma LiAlO_2$.

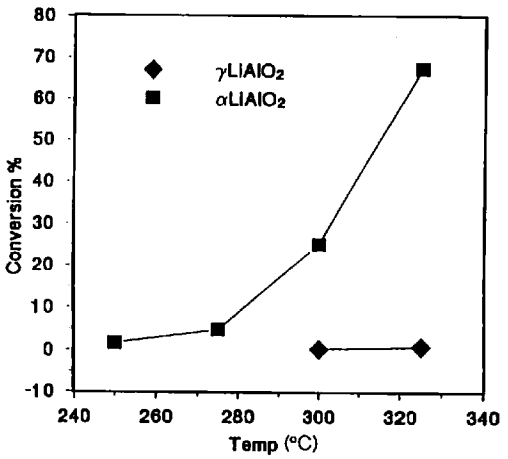

FIG. 3. Conversion versus temperature data of IPA over $\alpha LiAlO_2$ and $\gamma LiAlO_2$ at GHSVs of 71 and 83 hr^{-1}, respectively.

selectivity data in Fig. 4 reveals a different product distribution. $\gamma LiAlO_2$ has a ((ACET + C6 + AP) : (PROP)) ratio of 3 : 1 and $\alpha LiAlO_2$ has a ratio of 20 : 1. The ratios show that both $\alpha LiAlO_2$ and $\gamma LiAlO_2$ primarily exhibit base-catalyzed activity.

The differences in the selectivities of the base-catalyzed products serve as a measure of the relative strength of the basic sites within the range where reaction rates increase with base strength. The conversion of IPA to acetone (dehydrogenation) requires the abstraction of the hydroxyl proton (determined in solution, $pK_a \approx 18$) (20) by a basic site. As noted earlier, the C6 products produced from acetone were only observed on $\alpha LiAlO_2$. The base-catalyzed aldol condensation of acetone requires abstraction of an H_α (determined in solution, $pK_a \approx 20$) (20) by a basic site. The previously mentioned pK_a values do not indicate the strength of the basic site (H_0) needed to abstract a proton at reaction conditions. In an analysis of acetaldehyde aldol condensation (determined in solution, H_α, $pK_a \approx 17$ (21)) on MgO, CaO, and PbO, Kawaguchi *et al.* (22) found that condensation activity correlated with basic sites having a strength of $H_0 \approx 9.3$ as determined by indicator methods. Thus, the pK_a values from solution data can be used to approximate the *relative* difference in the strength of the basic sites. In our case it appears that the difference in the strength of the basic sites on $\alpha LiAlO_2$ and $\gamma LiAlO_2$ is at least two H_0 units with $\alpha LiAlO_2$ having the stronger basic sites.

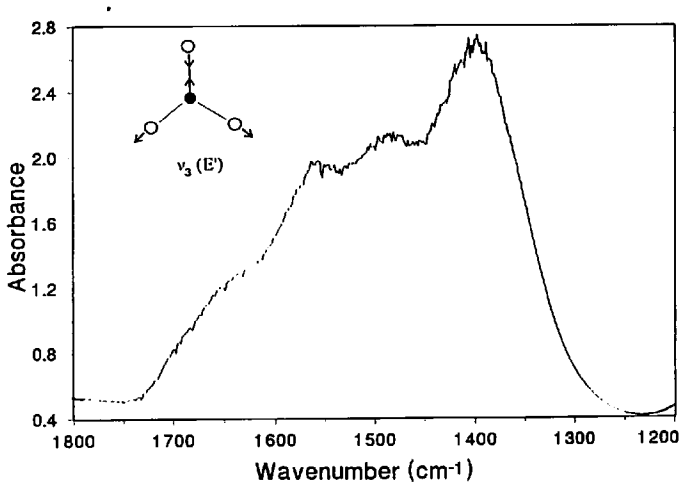

FIG. 2. The IR spectrum of adsorbed CO_2 on $\alpha LiAlO_2$ in the region of the ν_3 vibration (asymmetric stretch).

The catalytic data are consistent with a localized charge description of oxide anion basicity. Owing to the longer metal–oxygen bonds in the $M_{(oct)}$–O versus $M_{(tet)}$–O system ($Li_{(oct)}$–O = 2.12 Å and $Al_{(oct)}$–O = 1.90 Å (11); $Li_{(tet)}$–O = 2.00 Å and $Al_{(tet)}$–O = 1.76 Å (12)) and the more positive charge of the electrostatic bonds in the $M_{(tet)}$–O versus $M_{(oct)}$–O system, the surface oxide anions of $\alpha LiAlO_2$ would on average exhibit more negative charge (electron density) compared to $\gamma LiAlO_2$. In the charge localization model, the charge of an electrostatic bond is defined as the cation charge divided by cation coordination number (23). Based on this model, the basic sites of $\alpha LiAlO_2$ will be stronger than those of $\gamma LiAlO_2$, which is consistent with the selectivity data presented in Fig. 4. The comparison between α and γ $LiAlO_2$ clearly shows that $\gamma LiAlO_2$ does not possess basic sites of sufficient strength for acetone condensation. Recently, Dronskowski reported that the lithium cation in $\gamma LiAlO_2$ is a stronger Lewis acid compared to lithium in $\alpha LiAlO_2$ (24). The difference in acidity was attributed to the framework structure, therefore, consistent with our IPA results, $\alpha LiAlO_2$ is the stronger base.

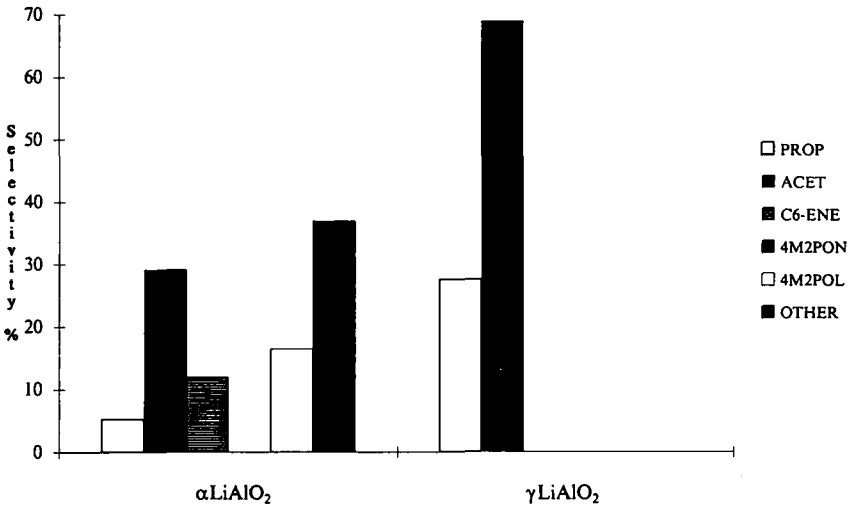

FIG. 4. IPA selectivity data of $\alpha LiAlO_2$ and $\gamma LiAlO_2$. $\alpha LiAlO_2$ parameters are T = 300°C, GHSV = 900 hr^{-1}, and conversion = 3.4%. $\gamma LiAlO_2$ parameters are T = 325°C, GHSV = 36 hr^{-1}, and conversion = 2.9%.

This comparison does not explain the variety of C6 products observed with $\alpha LiAlO_2$. A more informative comparison involving $\alpha LiAlO_2$ and calcined "$HAlO_2$" and a detailed discussion of the reaction pathways associated with the formation of the C6 products follows in the next section.

$\alpha LiAlO_2$ vs calcined "$HAlO_2$." One aspect of the comparison between $\alpha LiAlO_2$ and calcined "$HAlO_2$" was to examine the effect that a ten fold change in lithium concentration has on the basicity of these two materials. Comparison of conversion data, see Fig. 5, shows greater conversion on $\alpha LiAlO_2$, even though it has 33% less surface area. At 325°C and a GHSV ≈ 80 hr^{-1}, $\alpha LiAlO_2$ exhibited a conversion of 54.3% compared to 21.5% for calcined "$HAlO_2$."

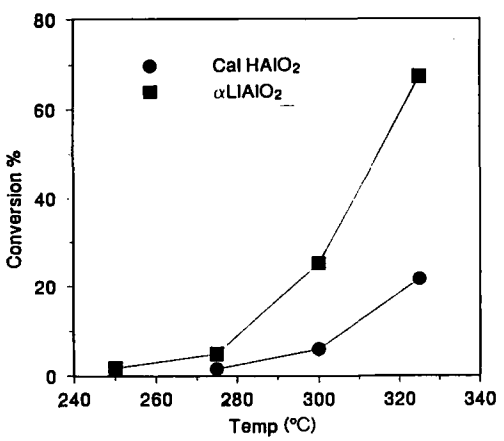

FIG. 5. Conversion versus temperature data of IPA over $\alpha LiAlO_2$ and calcined "$HAlO_2$" at GHSVs of 71 and 61 hr^{-1}, respectively.

A comparison of the selectivity patterns of $\alpha LiAlO_2$ and calcined "$HAlO_2$," see Fig. 6, at a similar conversion (27.2 and 21.5%, respectively) and temperature (T = 325°C, GHSV = 407 and 61 hr^{-1}, respectively) shows a marked increase in propylene selectivity from 3.5% for $\alpha LiAlO_2$ to 13.6% for calcined "$HAlO_2$." At a similar temperature and conversion, the yield of dehydration products varied inversely with the lithium concentration. A comparison of the ((ACET + C6 + AP) : (PROP)) ratios shows $\alpha LiAlO_2$ with a larger ratio than calcined "$HAlO_2$," 28.4 : 1 vs 6.4 : 1, which indicates that the surface of $\alpha LiAlO_2$ is more basic compared to calcined "$HAlO_2$."

The selectivity patterns presented in Fig. 6 show that the chemistry associated with the formation of the C6 products on both $\alpha LiAlO_2$ and calcined "$HAlO_2$" is not identical. The formation of 4M2PONE and 4M2POL is unique to $\alpha LiAlO_2$. This result indicates the presence of catalytic sites on $\alpha LiAlO_2$ not found on calcined "$HAlO_2$." In the next section, reaction sequences that describe the formation of the C6 products are presented.

Aldol condensation. Aldol condensation of two acetone molecules is the first in a series of steps that leads to the formation of the MO and 4M3PEN2OL, see Fig. 7. The first step in the base catalyzed aldol condensation is the abstraction of an H_α to form a carbanion and a surface proton (20). Second, the carbanion attacks the carbonyl carbon of another acetone molecule to form the alcoholate anion of DAA. Owing to the rapid dehydration to MO, only trace amounts of DAA were observed at these conditions (25). At the same conditions, MO is also very reactive, which explains its small concentration in the product mixture. MO most likely undergoes rapid

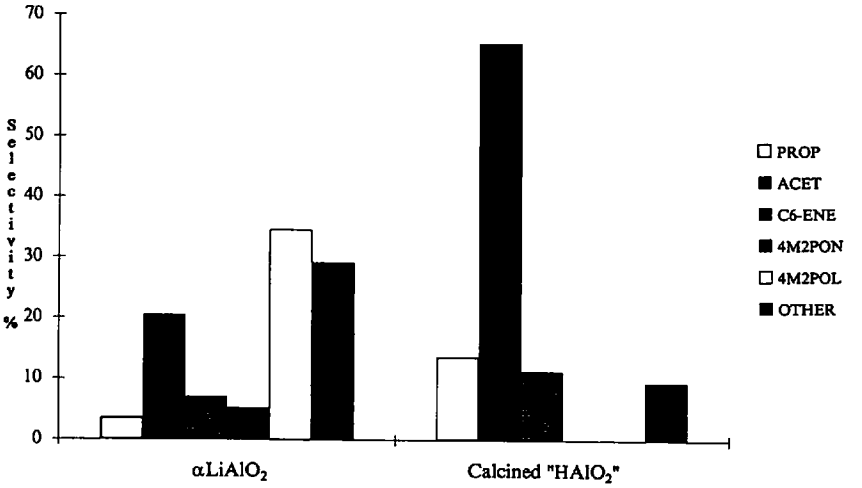

FIG. 6. IPA selectivity data of $\alpha LiAlO_2$ and calcined "$HAlO_2$." $\alpha LiAlO_2$ parameters are T = 325°C, GHSV = 407 hr^{-1}, and conversion = 27.2%. Calcined "$HAlO_2$" parameters are T = 325°C, GHSV = 61 hr^{-1}, and conversion = 21.5%.

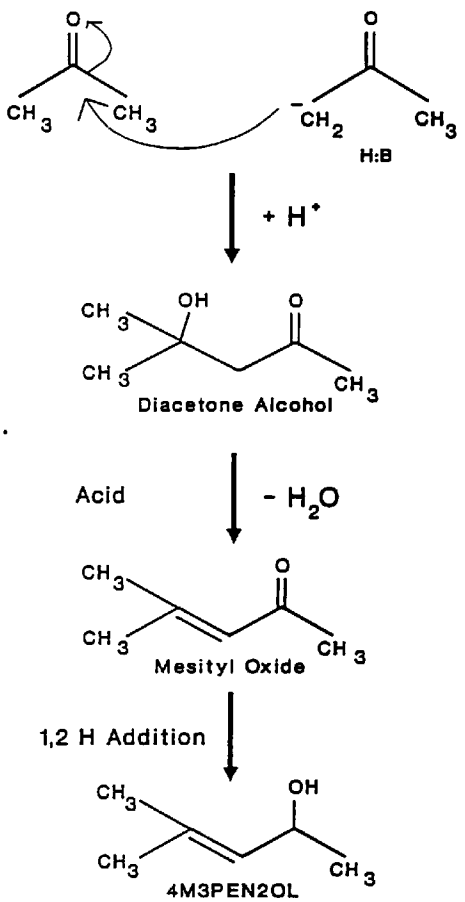

FIG. 7. A reaction pathway that describes the base catalyzed condensation of two acetone molecules to form 4-methyl-3-penten-2-ol.

conversion to its corresponding alcohol, 4M3PEN2OL (4-methyl-3-penten-2-ol), via a base catalyzed hydrogen transfer from IPA (6).

The reaction sequence that describes hydrogen transfer is similar to that for dehydrogenation. The first step requires the abstraction of a hydroxyl proton from IPA to form a 2-propoxy anion and a surface proton. The anion can transfer a hydride ion to the surface (dehydrogenation) or it can transfer a hydride ion to a proximal adsorbed ketone molecule (hydrogen transfer). GC/MS analysis of the product mixture of $\alpha LiAlO_2$ did not detect the presence of 4M3PEN2OL. It is known that allylic alcohols such as 4M3PEN2OL undergo rapid base and/or acid-base dehydration at the conditions used in the catalytic studies (26, 27). The product of either dehydration pathway is C6DIENE. Therefore, even though 4M3PEN2OL is not observed, its existence is consistent with the conversion of MO to C6DIENE.

4M3PEN2OL as the furcation point. In the comparison of $\alpha LiAlO_2$ and calcined "$HAlO_2$," it was shown that 4M2PONE and 4M2POL were only observed on $\alpha LiAlO_2$, while C6DIENE and AP were observed on both materials. The reaction sequences with 4M3PEN2OL as the furcation point that lead to all three identified C6 products are shown in Fig. 8. The first C6 reaction sequence discussed is alcohol dehydration. As mentioned in the aldol condensation section, 4M3PEN2OL can follow two dehydration pathways. The first pathway requires only basic sites and applies to β–γ unsaturated alcohols (27). The initial step involves removal of the hydroxyl proton to form an alkoxide anion. The oxygen of the alkoxide anion forms a bond with an H_δ to form a cyclic intermediate. This intermediate then expels the newly formed OH group and forms the

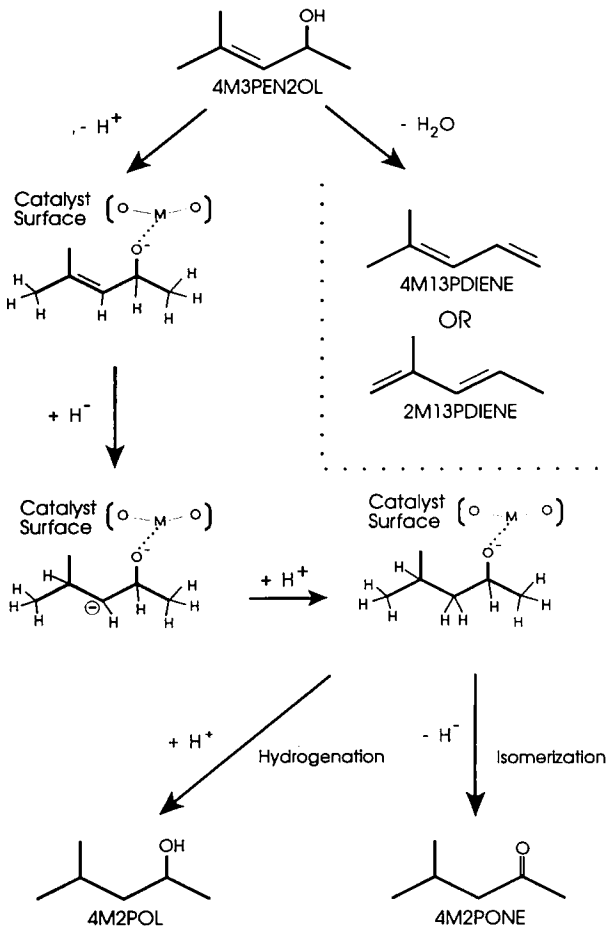

FIG. 8. A reaction pathway that describes the conversion of 4-methyl-3-penten-2-ol to 4-methyl-2-pentanone and 4-methyl-2-pentanol via hydride ion chemistry.

diene, 2-methyl-1,3-pentadiene. The other pathway proceeds via an acid–base pair catalyzed H_β elimination reaction that is analogous to the pathway for propylene formation from IPA (5). The product from this pathway is 4-methyl-1,3-pentadiene. Mass spectroscopy was not able to identify which isomer exists in this system.

The second C6 reaction sequence describes the conversion of 4M3PEN2OL to 4M2PONE and 4M2POL utilizing hydrogen transfer chemistry and surface H^+ and H^- species. In the work of Sharf *et al.*, the intermolecular transfer of hydrogen from IPA directly to the (C=C) positions of allylic aldehydes and ketones was not observed (28). Therefore, an intermolecular hydrogen transfer from 2-propoxy anion to the (C=C) position of 4M3PEN2OL can be ruled out. However, hydrogen addition to the C=C position does occur with our catalyst, and we propose that hydrogen addition is the result of a surface mediated transfer of H^- from an adsorbed alkoxy anion to the adsorbed unsaturated alcohol.

As noted earlier in the discussion of alcohol dehydrogenation, the 2-propoxy anion can transfer its hydride ion to the surface of the catalyst to form an $M^{+n} \cdots H^{\ominus}$ adduct and an adsorbed ketone (6) These *in situ* formed adduct sites are considered basic because of the electron donating ability of the hydride ion. Charge neutrality is preserved on the surface by the hydroxyl proton transferred to the oxygen anion during the initial step of alcohol dehydrogenation. It is believed that the hydride ion is stabilized on $\alpha LiAlO_2$ in the form of an $Li^+ \cdots H^{\ominus}$ adduct. Compared to the smaller aluminum cation (ionic radius = 0.54 Å, CN = 6) (29), the lithium cation (ionic radius = 0.76 Å, CN = 6) (29) on the surface is less screened by oxygens (30), which makes lithium the more likely cation to stabilize the H^- ion. Similarly, it is well known that lithium can form a stable hydride salt, LiH (31). In addition, the existence of a $Li^+ \cdots H^{\ominus}$ adduct seems reasonable based on the known information regarding sodium on alumina used as an olefin dehydrogenation catalyst. The active sites on this catalyst are $Na^+ \cdots H^{\ominus}$ adducts (27).

The first step in the proposed hydride pathway that leads to both 4M2PONE and 4M2POL from 4M3PEN2OL involves the dissociative adsorption of 4M3PEN2OL on the surface of $\alpha LiAlO_2$ to form an alcoholate anion and a surface proton; see Fig. 8. This anion can undergo a hydride attack at C_γ to form a dianion that contains a 2° carbanion (32). Hydride attack at the C_β position was excluded because of the instability of the dianion that contains a 3° carbanion. The dianion formed from the addition of hydride to C_γ can accept a proton at C_β to form the alcoholate anion of 4M2POL which can transfer its H_α (hydride ion) to the surface or to a proximal ketone adsorbed on the surface. The product of this hydride ion loss is 4M2PONE (isomerization); see Fig. 8. However, the adsorbed alcoholate anion can abstract a proton from the surface to form 4M2POL (hydrogenation); see Fig. 8.

Based on the selectivity data for $\alpha LiAlO_2$ (Table 3), hydrogenation is favored over isomerization. At 325°C and a GHSV = 71 hr^{-1}, the selectivities for the isomerization and hydrogenation products are 7.4 and 17.0%, respectively. These results are consistent with the those of Hubaut *et al.*, where it was reported that hydrogenation was favored over isomerization for a series of allylic alcohols studied with a copper chromite catalyst (33). The description of the reaction sequences leading to 4M2PONE and 4M2POL highlights the complexity of the reaction chemistry of IPA, but it also emphasizes the added utility of the IPA reaction for the characterization of mixed metal oxides.

We believe that the difference in the selectivity data of $\alpha LiAlO_2$ and calcined "$HAlO_2$" is the result of the formation of $Li^+ \cdots H^{\ominus}$ adduct sites on $\alpha LiAlO_2$. Calcined "$HAlO_2$" also contains a significant concentration of lithium, but differences in cation coordination appear to affect the ability of lithium to form the adduct site. Based

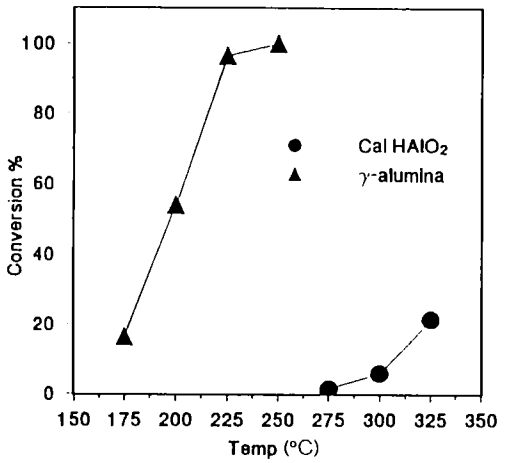

FIG. 9. Conversion versus temperature data of IPA over calcined "$HAlO_2$" and γ-alumina at GHSVs of 61 and 84 hr^{-1}, respectively.

on the known information concerning the structure of "$HAlO_2$" (1–3, 13, 14), the probable locations for the lithium cations in calcined "$HAlO_2$" are tetrahedral sites. Conclusions based on the catalytic data of $\gamma LiAlO_2$ suggest that metal oxides where lithium is in tetrahedral coordination are less active for base catalysis.

In summary, we propose two reaction sequences to explain the formation of the C6 products on calcined "$HAlO_2$" and $\alpha LiAlO_2$. Both sequences originate from the same molecule 4M3PEN2OL. The sequence which leads to the base and/or acid–base dehydration product (C6DIENE) was found to occur on both materials. The other sequence which leads to the isomerization (4M2PONE) and the hydrogenation (4M2POL) products was found to occur only on $\alpha LiAlO_2$.

Calcined "$HAlO_2$" vs γ-alumina. The purpose of the comparison of IPA catalytic data of calcined "$HAlO_2$" and γ-alumina is to examine the effect that a small amount of lithium has on the alcohol dehydration activity of an aluminate. The catalytic data presented in Fig. 9 shows a significant difference in the activity observed on calcined "$HAlO_2$" and γ-alumina. γ-Alumina exhibited moderate activity (16.5%, T_{rxn} = 175°C) at a temperature 100°C lower than the temperature of initial activity (1.5%, T_{rxn} = 275°C) observed on calcined "$HAlO_2$." These findings indicate that the residual lithium in calcined "$HAlO_2$" (Li : Al ratio = 1 : 10) markedly reduces the alcohol dehydration activity. The dominant factor in alcohol dehydration is the strength of the acidic sites. As expected, the "alkali-free" sample exhibited only dehydration selectivity; see Table 6. DIPE formation is also considered dehydration. The selectivity data of calcined "$HAlO_2$" shown in Table 5 reveals a significantly different selectivity pattern. The character of the sample as described by the ((ACET + C6 + AP) : (PROP)) ratio, 6.4 : 1, at T_{rxn} = 325°C and GHSV = 61 hr^{-1} is predominantly basic. This result indicates that the lithium cations neutralize the strong acidic sites that are important for low temperature (<200°C) alcohol dehydration activity and are responsible for the formation of basic sites.

These conclusions agree with those found in the literature. In a catalytic study of activated alumina impregnated with sodium (NaOH or NaCl, Na : Al = 1 : 29), Pines and Haag showed that the alkali metal cation had a dramatic effect on acid catalyzed activity (19). 3,3-dimethyl-1-butene isomerization was not observed on the alkali impregnated samples versus 97.3% conversion for the alkali-free sample (LHSV = 2.0 hr^{-1}, T_{rxn} = 350°C). In addition, it was reported that the alkali-free samples exhibited 82% conversion for 1-butanol dehydration where the sample that contained alkali exhibited only 3% conversion (LHSV = 2.0 hr^{-1}, T_{rxn} = 350°C). In both cases, the effects of the alkali on the acid catalyzed activity of the aluminas was attributed to the neutralization of the acidic sites by sodium cations.

TPD Data

$\alpha LiAlO_2$ vs $\gamma LiAlO_2$. A comparison of the TPD profiles, see Fig. 1, of $\alpha LiAlO_2$ and $\gamma LiAlO_2$ indicates a dramatic difference in the strength and number of the basic sites. Both catalysts exhibit desorption peaks centered at 80–100°C, but only $\alpha LiAlO_2$ has desorption peaks at higher temperatures. The data shown in Table 1 show $\alpha LiAlO_2$ with a base site density of 5.2×10^{-6} mole m^{-2} and $\gamma LiAlO_2$ with a base site density of 1.7×10^{-6} mole m^{-2}. These results show that the "basicity" (strength and number of sites) of $\alpha LiAlO_2$ is greater than that of $\gamma LiAlO_2$. This is consistent with the findings from the IPA reaction data which showed that both catalysts were active for dehydrogenation but only $\alpha LiAlO_2$ was active for acetone aldol condensation. As pointed out earlier, it requires a stronger base to remove the H_α of acetone than the hydroxyl proton of IPA.

$\alpha LiAlO_2$ vs calcined "$HAlO_2$." The TPD profiles of $\alpha LiAlO_2$ and calcined "$HAlO_2$" show multiple basic sites. In addition, the position of the highest temperature desorption peak is approximately 300°C. These results indicate that the distribution by strength of the basic sites is similar. The base site densities of $\alpha LiAlO_2$ and calcined "$HAlO_2$" are 5.6×10^{-6} and 1.2×10^{-6} mole m^{-2}, respectively. The desorption profiles and densities are similar to other mixed-metal oxides (9). Hence, differences in the selectivity results (only $\alpha LiAlO_2$ showing reduction of 4M3PEN2OL) do not appear to depend on differences in the strength or density of the basic sites.

IR Data

Because of its D_{3h} symmetry, the free carbonate ion has one Raman active vibration at 1063 cm^{-1} (ν_1 (A_1'); symmetric stretch), one IR active vibration at 879 cm^{-1} (ν_2 (A_2''); out-of-plane deformation), and two E vibrations at 1415 cm^{-1} (ν_3; asymmetric stretch) and at 680 cm^{-1} (ν_4; in-plane deformation) which are IR and Raman active (34). Coordination lowers the symmetry, splitting the doubly degenerate ν_3 and ν_4 vibrations and activating ν_1 in the IR (34, 35). Chemisorbed carbonate species are generally identified on the basis of the splitting of the ν_3 vibration, $\Delta\nu_3$ (34, 35). Average values of $\Delta\nu_3$ have been tabulated from compounds whose structures are known through other methods such as X-ray diffraction. A $\Delta\nu_3$ of 100 cm^{-1} is the average value for monodentate carbonate structures. A $\Delta\nu_3$ of 300 cm^{-1} is the average value for bidentate coordination, and a $\Delta\nu_3$ of 400 cm^{-1} or higher is indicative of a bridged carbonate. $\alpha LiAlO_2$ exhibits four IR bands in the ν_3 region 1408, 1491, 1560, and 1645 cm^{-1}. Consistent with the TPD, the spectrum clearly indicates several carbonate species in different surface environments on $\alpha LiAlO_2$.

CONCLUSIONS

In this paper it has been shown that the IPA probe reaction can be used to demonstrate the effect of cation coordination on the basicity of mixed-metal oxides. Owing to its basic character, $\alpha LiAlO_2$ was capable of aldol condensation, whereas $\gamma LiAlO_2$ was not. FTIR and CO_2 TPD results indicated a difference in the strength of the basic sites of $\alpha LiAlO_2$ and $\gamma LiAlO_2$ with the latter having one site which weakly binds CO_2. This is in contrast to the broad desorption peaks observed in the TPD profile of $\alpha LiAlO_2$ and calcined "$HAlO_2$" which indicate multiple sites that strongly chemisorb CO_2. Clearly the basicities of $\alpha LiAlO_2$ and $\gamma LiAlO_2$ are markedly different, that is $\gamma LiAlO_2$ with cations in tetrahedral coordination is the weaker base compared to $\alpha LiAlO_2$ with cations in octahedral coordination. This finding provides strong evidence in support of cation coordination effects on basicity in mixed-metal oxides. Recognizing the unique solid-state chemistry of $\alpha LiAlO_2$ (1), we cannot eliminate, as a contributing factor, the possibility of near-surface ion exchange. Nonetheless, those features inherent to the bulk will affect the concentration and the coordination of the ions at the surface. From a comparison of both $\alpha LiAlO_2$ and calcined "$HAlO_2$" selectivity data, it was shown that $\alpha LiAlO_2$ had unique active sites for the conversion of 4M3PEN2OL which led to the formation of both 4M2PONE and 4M2POL. The development of a reaction scheme describing the formation of both 4M2PONE and 4M2POL was used to show that the active sites unique to $\alpha LiAlO_2$ most likely consist of $Li^+ \cdots H^{\ominus}$ adducts formed *in situ* during alcohol dehydrogenation. The conclusion reached from a comparison of both calcined "$HAlO_2$" and γ-alumina activity and selectivity data was that the residual lithium in calcined "$HAlO_2$" decreases alcohol dehydration activity and is responsible for the formation of basic sites.

ACKNOWLEDGMENTS

The authors gratefully acknowledge support from the Department of Energy, Contract DE-F605-86ER75295, for the surface area and porosity measurement equipment, and from the National Science Foundation, Solid State Chemistry, Contract DMR-8915897, for support on compound precursors to mixed metal oxides. We also express thanks to Professor Herman Pines, Professor Robert Burwell, Dr. Werner Haag, and Professor Martin Johnson for their invaluable comments regarding the development of the reaction pathways.

REFERENCES

1. Poeppelmeier, K. R., and Kipp, D. O., *Inorg. Chem.* **27,** 766 (1987).
2. Kipp, D. O., "Cation Replacement in Lithium Aluminum Oxide." Thesis, Northwestern University, Evanston, 1988.
3. Tomczak, D. C., Thong, S. H. K., and Poeppelmeier, K. R., *Catal. Lett.* **12,** 139 (1992).
4. Figlarz, M., *Chem. Scr.* **28,** 3 (1988).
5. Pines, H., and Manassen, J., *Adv. Catal.* **167,** 49 (1966).
6. Kibby, C. L., and Hall, W. K., *J. Catal.* **31,** 65 (1973).
7. Pepe, F., and Stone, F. S., *J. Catal.* **56,** 160 (1979).
8. Krylov, O. V., "Catalysis by Non-Metals." Academic Press, New York, 1970.
9. McKenzie, A. L., Fishel, C. T., and Davis, R. J., *J. Catal.* **138,** 547 (1992).
10. Kurokawa, H., Kato, T., Kuwabara, T., Ueda, W., Morikawa, Y., Moro-Oka, Y., and Ikawa, T., *J. Catal.* **126,** 208 (1990).
11. Marezio, M., and Remeika, J. P., *J. Phys. Chem.* **44,** 3143 (1966).
12. Marezio, M., *Acta Crystallogr.* **19,** 396 (1965).
13. Thong, S. H. K., "Cation Replacement in the Rocksalt Structure." Thesis, Northwestern University, Evanston, 1990.
14. Tomczak, D. C., "Catalytic Characterization of Lithium Aluminum Oxides; Including a Study of Both the Cation Replacement Chemistry and the Structure of the $\alpha LiAlO_2$/"$HAlO_2$" System." Thesis, Northwestern University, Evanston, 1993.
15. Brunauer, S., Emmett, P. H., and Teller, E., *J. Am. Chem. Soc.* **60,** 309 (1938).
16. Lippens, B. C., and De Boer, J. H., *J. Catal.* **4,** 319 (1965).
17. Eucken, A., and Heuer, K., *Z. Phys. Chem.* **196,** 40 (1950).
18. Drezdon, M. A., *in* "Novel Materials in Heterogeneous Catalysis" (T. K. Baker and L. L. Murrell, Eds.), Symposium Series No. 437, p. 140. American Chemical Society, Washington, DC, 1990.
19. Pines, H., and Haag, W., *J. Am. Chem. Soc.* **82,** 2472 (1960).
20. House, H. O., "Modern Synthetic Reactions." Benjamin Cummings, London, 1972.
21. Streitwieser, A., and Heathcock, C., "Introduction to Organic Chemistry." Macmillan, New York, 1985.
22. Kawaguchi, T. Haegawa, S., Morikawa, S., and Suzuki, H., Paper No. 3, presented at the Meeting of the Catalysis Society of Japan, Sendai, 1968.
23. Knozinger, H., and Ratnasamy, P., *Catal. Rev.-Sci. Eng.* **17,** 31 (1978).
24. Dronskowski, R., *Inorg. Chem.* **32,** 1 (1993).
25. Kubelkova, L., Cejka, J., and Novakova, J., *Zeolites* **11,** 31 (1978).

26. Schachter, Y., and Pines, H., *J. Catal.* **11,** 147 (1968).
27. Pines, H., and Stalick, W. M., "Base-Catalyzed Reactions of Hydrocarbons and Related Compounds." Academic Press, New York, 1977.
28. Sharf, V. Z., Friedlin, Kh. L., and Vorob'eva, N. K., *Izv. Akad. Nauk SSSR Ser. Khim.* **8,** 1846 (1972).
29. Shannon, R. D., *Acta Crystallogr. Sect. A* **32,** 751 (1976).
30. Jensen, W. B., "The Lewis Acid-Base Concepts." Wiley, New York, 1980.
31. Cotton, F. A., and Wilkinson, G., "Advanced Inorganic Chemistry," 5th ed. Wiley, New York, 1988.
32. Dimmel, D. R., Fu, W. Y., and Ghapure, S. B., *J. Org. Chem.* **41,** 3092 (1975).
33. Hubaut, R., Daage, M., and Bonnelle, J. P., *Appl. Catal.* **22,** 243 (1986).
34. Busca, G., and Lorenzelli, V., *Mater. Chem.* **7,** 89 (1982).
35. Nakamoto, K., Fujita, J., Tanaka, S., and Kobayaski, M., *J. Am. Chem. Soc.* **79,** 4904 (1957).